Satellite-based Hurricane Risk Assessment for Roadways via Vegetation 3D Modeling and Building Detection

Michele Gazzea
Department of Computer Science and Electrical Engineering
Western Norway University of Applied Sciences, Bergen, Norway
Email: michele.gazzea@hvl.no

Alican Karaer
Department of Civil and Environmental Engineering
FAMU–FSU College of Engineering
2525 Pottsdamer Street, Tallahassee, FL 32310
Email: akaraer@fsu.edu

Mahyar Ghorbanzadeh
Department of Civil and Environmental Engineering
FAMU–FSU College of Engineering
2525 Pottsdamer Street, Tallahassee, FL 32310
Email: mghorbanzadeh@fsu.edu

Eren Erman Ozguven
Department of Civil and Environmental Engineering
FAMU–FSU College of Engineering
2525 Pottsdamer Street, Tallahassee, FL 32310
Email:ozguvene@gmail.com

Reza Arghandeh
Department of Computer Science and Electrical Engineering
Western Norway University of Applied Sciences, Bergen, Norway
Email: arghandehr@gmail.com

Word Count: 4698 words + 0 tables (250 words per table) = 4698 words (7500 words max)
Submitted for presentation [30 July 2021]

Abstract

Infrastructures such as roadways, power lines, and communications networks play a critical role in our society. However, they are also susceptible to failures, especially after natural events, easily affecting large geographical areas. Predicting where and when these failures will occur with high confidence is very difficult due to the stochastic nature of such events. Nevertheless, it is possible to know which areas are more vulnerable in advance and plan accordingly. This paper aims to use just remote sensing techniques based on satellite images to detect roadways vulnerabilities to hurricanes. The framework exhibits a modular architecture that enables detecting and mapping in 3D vegetation and detecting buildings. We propose a risk function based on the information retrieved from the satellite image which can be used to create a risk map of the area. The study area has been selected in Tallahassee, Florida where a high-resolution satellite image has been acquired in September 2018, before Hurricane Michael main hit. The findings of this work can help the management teams and city responders to identify the most vulnerable regions which are under the risk of disruption and to organize the resources prior to the event. The advantages of our approach are that the entire framework can be use as a end-to-end standalone solution for risk analysis at city level and can be easily expanded with other source of data.

Keywords: Remote Sensing, Satellite Imagery, Hurricane Vulnerability Assessment

1 Introduction

Our modern society relies on critical infrastructures to support all the operations, functionalities and enterprises. Such infrastructures are composed of public and private physical structures such as roads, railways, bridges, tunnels, water supply, sewers, electrical grids, and telecommunications connectivity [1]. Such fundamental elements are often exposed to failures and disruptions, dramatically affecting citizens' life and causing stress on the society. Thus, it is fundamental to understand and monition the vulnerability of such infrastructures to ease or limit outages' consequences. Disruptions can be caused by various events, from technical failures (electric outages, traffic indents) to natural disasters (floods, landslides, hurricanes, wildfires, earthquakes, etc). While accidents and technical failures may have limited extents, disruptions caused by nature may cover large areas. Among the different infrastructures, the road network is critical for transportation and all services' accessibility and it is severely affected by natural disasters like hurricanes.

Hurricanes and the damages caused by them have gained attention in recent years [2], with vegetation being the first cause of roadway closures [3]. In [4], the authors developed a framework to automatically detect fallen trees after a hurricane using remote sensing images. Moreover, some studies, as [5], [6] and [7] tried to quantify the tree failure probability after extreme weather events proposing empirical models to estimate the possibility of trees failures.. Such works often try to predict the tree crown and other estimated parameters [8] and combine them with wind data. However, a major challenge in estimating the consequences of tree failure in a city scale is to obtain the tree parameters. For example, it is impractical to survey by manual or visual inspection all trees in a city to obtain the required tree parameters. Aerial images are a valuable source of data for hurricane damage assessment [9]. However, helicopters high operating costs and drones' limited coverage are a burden on large scale applications. In recent years, the dramatic drop in satellites' launching cost and the growing number of satellites in orbit significantly reduced the cost of high-resolution satellite imagery [10]. Commercial satellite providers can offer very high-resolution images (0.3 to 0.5 pixels/meter) with a high revisiting frequency for most parts of the globe. Furthermore, single snapshots can cover large portions at once. Therefore, the combination of coverage, frequency, and cost-efficiency of satellite imagery in addition to advancements in machine learning creates a paradigm change for smarter cities enhancing situational and risk awareness for infrastructure network [11]. The notion of *risk* is adopted from [12], who propose that the results of a risk analysis should contain the description of a particular scenario, the probability of that scenario occurring, and the impact of the scenario. In other words, given a failure or outage, both the probability of its cause and the consequences of its effect should be taken into account. Following [13], the impact for users under a certain disruption scenario is referred to as the exposure of the user to that scenario.

In this paper, we propose a framework for risk and vulnerabilities detection along roadways using solely high-resolution satellite images. The framework is composed of three modules. The first deals with the cause of failure and automatically monitors the vegetation along roadways, giving important clues such as its density and height. The second one detects the building footprints and their density, dealing this way with the exposure aspect. Finally, this information are merged in the third sub-module into a risk function. A risk map can then be created for an entire area showing the vulnerable locations more prone to disruptions. The advantage of our approach is that, once the single modules are trained, the entire framework can be use as a end-to-end standalone solution for risk analysis at city level. Furthermore, given the modularity of its architecture, it can be easily expanded with other source of data.

2 Study Area and Data Description

Hurricane Michael was one of the strongest storms which hit the Southeast coast of the United States. It made landfall as a Category 5 hurricane in the Florida Panhandle region with maximum sustained wind speeds of 140 knots (161 mph) bringing catastrophic storm surge to the Florida State and Big Bend areas (especially Mexico Beach and Panama City) [14]. It hit Florida on October 10^{th} 2018, the related power outages affected nearly 400,000 electricity customers in Florida at their greatest extent, representing about 4% of the state [15]. Furthermore, damage to over 2.8 million acres (1.1 million hectares) of forested land caused an estimated $1.29 billion in damage to the timber industry. 12% of damaged forest area was classified as "catastrophic" by the Florida Forest Service [16]. Estimated damage from Michael throughout the United States reached $25 billion [17].

As a medium-sized city and the state capital, Tallahassee has a population of 193,551 as of the year 2018. It is also the home for two major universities, namely Florida State University (FSU) and Florida Agricultural and Mechanical University (FAMU). As a result, students comprise more than 35% of the entire population [18]. More than 30 state government agency headquarters, including the Capitol Building, Florida Supreme Court and Florida Governor's Mansion are located in Tallahassee. As such, the City of Tallahassee was selected for the proposed case study.

One high-resolution multi-spectral satellite image has been acquired for a 6 Km2 (2.3 mi2) portion of Tallahassee as shown in Figure 1. The image, provided by Maxar WorldView-2 satellite, is composed of four channels: red (R), green (G), blue (B) and near-infrared (NIR) with a spatial resolution of 0.5 meters/pixel. The given resolution allows to easily recognize trees, buildings and other infrastructure. The image is encoded as a GeoTIFF file, so each pixel can be precisely located in a geographical reference system.

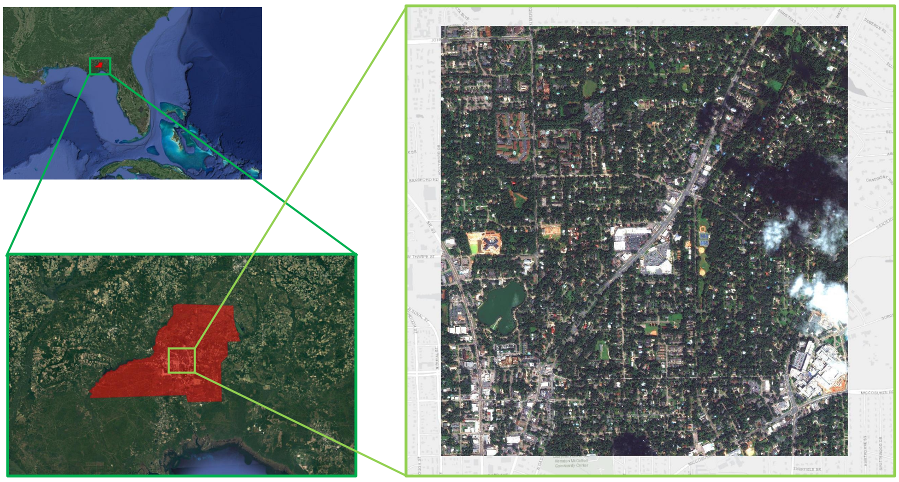

Figure 1: Study area located in the city of Tallahassee, the capital of Florida. A high-resolution satellite image has been acquired in September 14th 2018, few weeks before Hurricane Michael's main hit.

To build and validate the detection modules inside the framework, ground truth dataset from different sources have been used. We used Laser Imaging Detection and Ranging (LiDAR) point clouds to generate Digital Surface Models (DSM) of the area and to label trees (Figure 2).

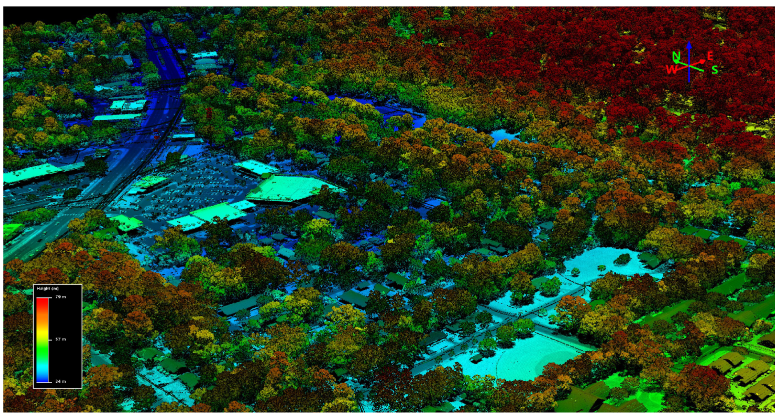

Figure 2: LiDAR point cloud for a portion of the study area. Point clouds have been used to generate the surface models for training and validating the vegetation detection algorithms.

The dataset is then used to train our segmentation models based on satellite images. LiDAR is a reliable tool capable of mapping an environment and providing the corresponding 3D point cloud representation but it is also very expensive and generate a huge amount of data that needs to be processed. The idea in our approach is to use available LiDAR data to train a suitable deep-learning model. Once the model is trained, LiDAR data is no longer needed. To train the building footprint detector we used a shapefile freely available for the city of

Tallahassee [19]. To display roadways and their characteristics, a vectorial shapefile was also downloaded from the municipality database. Roads are classified by importance as National, County and common roads.

3 Methodology

In this paper we aim to assess vulnerabilities along roadways using solely satellite images. As discussed in the introduction, the risk $\mathscr{R}$ associated to a failure is a combination of exposure $\mathscr{E}$ (how the disruption affect the users) and the probability of failure in a given scenario $\mathscr{P}$. In our study, we identify the vegetation as the primary cause of roadway closure (with fallen trees or tree debris) and the road importance and amount of buildings (both private and public) surrounding a road sector as a level of impact of such closure (Equation 1).

$$\mathscr{R} = \underbrace{(\text{building density; road importance})}_{\mathscr{E}} \otimes \underbrace{(\text{vegetation characteristics})}_{\mathscr{P}} \tag{1}$$

The building density can be used as a proxy to infer how many people live in a certain area or the amount of activities, giving a clue about the exposure of a failure. Equation 1 claims that, even if a piece of road is surrounded by many high vulnerable trees, the associated risk can still be low if nobody lives in the surroundings, reinforcing what is also expected from common sense. Therefore, given these considerations, our framework is composed by three modules. The first automatically monitors the vegetation along roadways, giving important clues such as its density and height. The second one detects the building footprints and their density. This information are merged, together with the prior knowledge about road importance, in the third sub-module into a risk function. A risk map can then be created for an entire area showing the vulnerable locations which are more prone to disruptions. The overall pipeline is shown in Figure 3 and each module further described in the following.

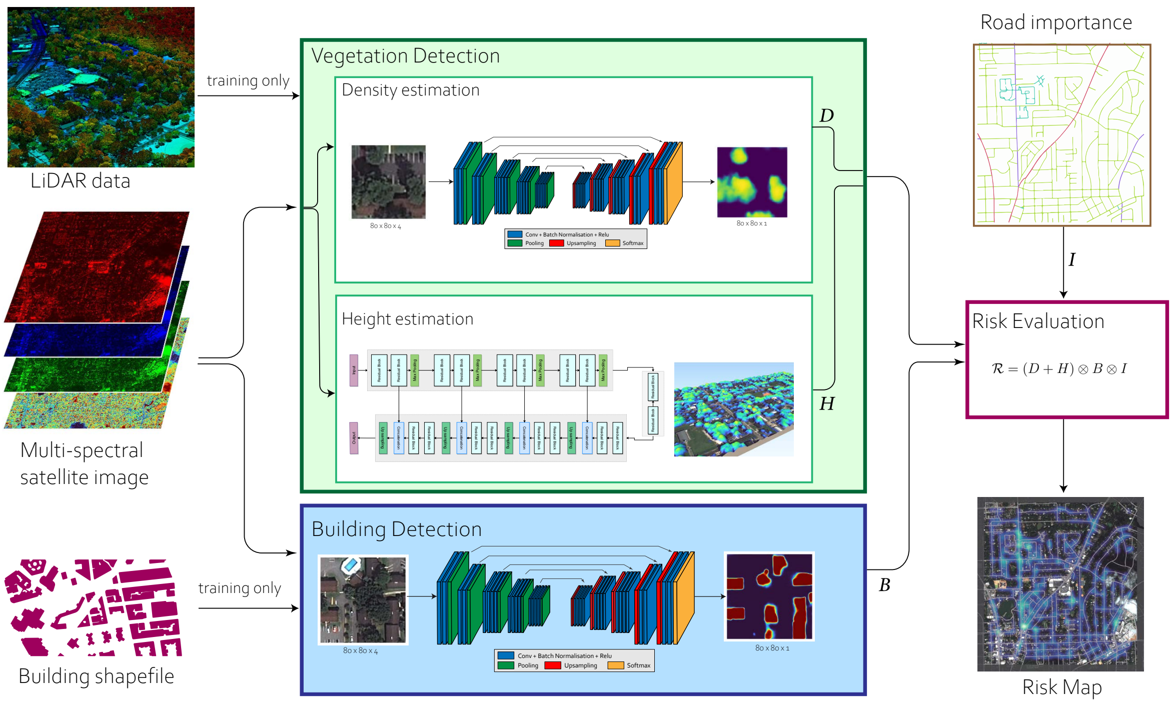

Figure 3: Overall pipeline of our approach.

3.1 Vegetation detection

The first module deals with vegetation, which is the main cause of roadways closures after hurricanes. High trees pose significant threat as, subjected to the strong winds, can easily fall on the road corridor. Furthermore, locations with a high number of trees are also dangerous as, from a probabilistic point of view, it is more likely that some of them may fall. Therefore, both density and height of trees are important factors to be taken into account for a risk analysis. Here we design two sub-modules to detect both of them using satellite images.

3.1.1 Density estimation

To detect the presence of trees we design a tree segmentation algorithm. Given the 4-channel (RGB-NIR) input image I, the corresponding output is a single-channel image where trees are detected. To perform the tree segmentation task, we use LiDAR data available for the considered study area for training. Although having LiDAR data makes the task easier, it is not strictly required to have such data for training. Since trees are easily and visually recognizable from satellite images, even by non-experts, a training dataset can be manually created as well. We use an encoder-decoder based architecture [20] as segmentation model. The architecture is composed by a cascade of $[16, 32, 64, 128, 256]$ convolutional layers activated by a *relu* activation function, followed by a batch normalization layer and a Max Pooling layer. Binary cross entropy $\mathscr{L}$ is used as loss function for training the network since only two labels are considered (0 for *no-trees* and 1 for *trees*). Such loss is often used in binary classification tasks and it is defined as

$$\mathscr{L} = -(y\log(p) + (1-y)\log(1-p)) \tag{2}$$

where p is the predicted probability value and $y = \{0, 1\}$ is the true label. The output of the model is a probability value between 0 and 1. Cross-entropy loss increases as the predicted probability diverges from the actual label. The architecture is shown in Figure 4.

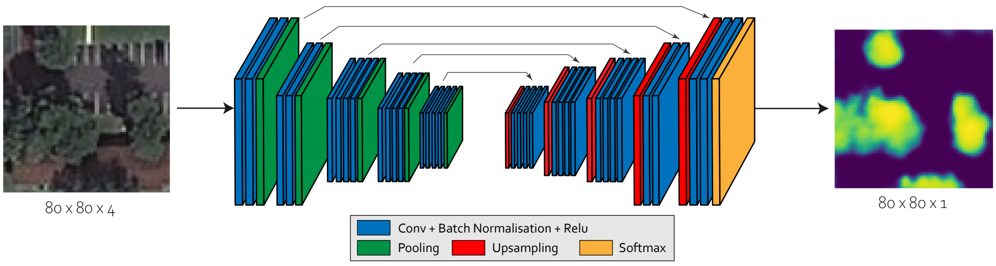

Figure 4: Architecture used for trees segmentation model. Given a satellite RGB-NIR image as input, the corresponding output is a mask where trees are detected. The output map is displayed as color-coded probability values of a pixel being part of a tree, from purple (no-tree) to yellow (tree).

3.1.2 Height estimation

This module estimates the tree canopy height from the satellite image. Measuring tree canopy height accurately from single images is a very challenging task because there are intrinsic ambiguities in mapping a color measurement into a height value. Usually the most common techniques for 3D generation include stereo images [21], multi-angular photogrammetry [22], SAR interferometry [23], and LiDAR [24]. Nevertheless, the main idea is to use satellite images and LiDAR data to train a model to learn the complex relationship between contextual information and canopy height. The trained model can then estimate the tree height in other areas to create a digital surface model from monocular images. Mathematically, we denote with y_i the true height of a pixel obtained from the ground-truth (LiDAR in our study) and $\hat{y}_i = f(x, \theta)$ the predicted height obtained from the model with parameters θ using the input image x. We formulate the task as a regression problem and we define a loss function as the mean squared error between the true height and the predict height:

$$\mathscr{L}(y, \theta, x) = \frac{1}{N}\sum_{i=1}^{N}(y_i - \hat{y}_i)^2 = \frac{1}{N}\sum_{i=1}^{N}\Big(y_i - f(x_i, \theta)\Big)^2 \tag{3}$$

A suitable model should minimize this loss function. Therefore, given a training dataset $\{x, y\}$, we aim to learn the weights of the model such that $\theta^* = \arg\min_\theta \mathscr{L}(y, \theta, x)$ Given the complexity of such a regression task, in this paper we use a neural network-based model called Res-UNet [25] (see Figure 5).

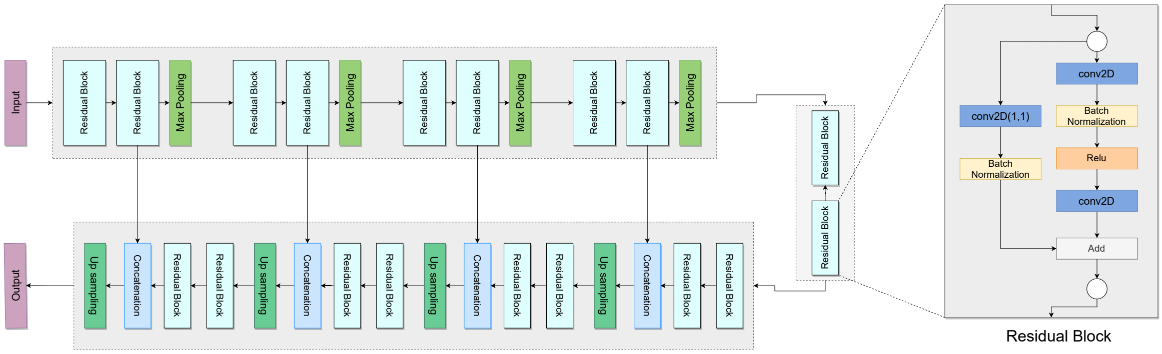

Figure 5: Architecture of the proposed Res-UNet model

It uses the popular U-net made for semantic segmentation as backbone where the traditional convolutional blocks have been replaced by residual blocks. Residual blocks have been first introduced in [26] to solve some difficulties in training deep neural networks and cope with the vanishing gradient issues. Traditionally, when an architecture goes too deep, gradient may degrade and the model stops to learn because the back-propagation chain is halted. Thus the residual block add a shortcut in the convolutional chain to prevent this issue. The architecture is composed by a cascade of $[16, 32, 64, 128, 256]$ residual blocks, consisting of convolutional layers, batch normalization and *relu* activation. The final layer of the decoder is connected to a Dropout layer and then activated by a sigmoid function.

3.2 Building footprint detection

To detect buildings from images, we make use of the same architecture and loss presented in 3.1.1 for semantic segmentation, where the ground truth is provided by a shapefile provided by the municipality of Tallahassee. The architecture is shown in Figure 6.

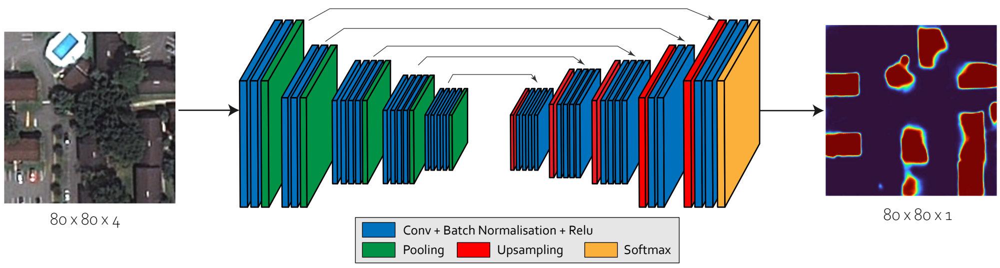

Figure 6: Architecture used for building detection. Given a satellite RGB-NIR image as input, the corresponding output is a mask where buildings are detected. The output map is displayed as color-coded probability values of a pixel being part of a building, from purple (no-building) to red (building).

3.3 Risk evaluation

Considering Equation 1, we aim to calculate a risk function which takes into account both the exposure and the probability of an outage. The vegetation density, height and building density are estimated from the satellite-based modules described before. The road importance is derived from the road shapefile. Therefore, given a certain location l along a road, we propose the following risk function $\mathscr{R}_l$:

$$\mathscr{R}_l = (D_l + H_l) \otimes B_l \otimes I_l \tag{4}$$

where D_l is the density of trees in l, H_l is the highest tree in l, B_l is the building density and I_l is the importance of the road whose l belongs to. The parameters are computed as follows.

- The tree density index D is computed as the ratio between the number of pixels belonging to the *tree* class and the total number of pixels in a window centered at l. It is a number between 0 and 1.

- the height index H is computed as the highest value retrieved from the Digital Surface Model in the a window centered at l and divided by 30 meters, which is the value of the highest trees in the area. It is a number between 0 and 1.
- The building density index B is computed as the ratio between the number of pixels belonging to the *building* class and the total number of pixels in a window centered at l. It is a number between 0 and 1.
- The road importance is a multiplier defined as $1, 1.5, 2$ for a *Common*, *County* and *State* road respectively.

4 Results and Discussion

We first trained and tested the different modules separately. The models have been developed using the Tensorflow/Keras libraries and has been trained using a NVIDIA RTX 2080 Super. QGIS has been used to visualize and integrate all different data. For the deep-learning training procedures we used the Adam optimizer with a learning rate of 0.001 for the segmentation tasks (i.e. vegetation and building density) and a learning rate of 10^{-4} for the regression task (i.e. height estimation). We also used an early stopping callback, which monitors the validation loss, to keep track of the loss and eventually stop the training to avoid over-fitting. Figure 7 shows the training and validation for the three modules.

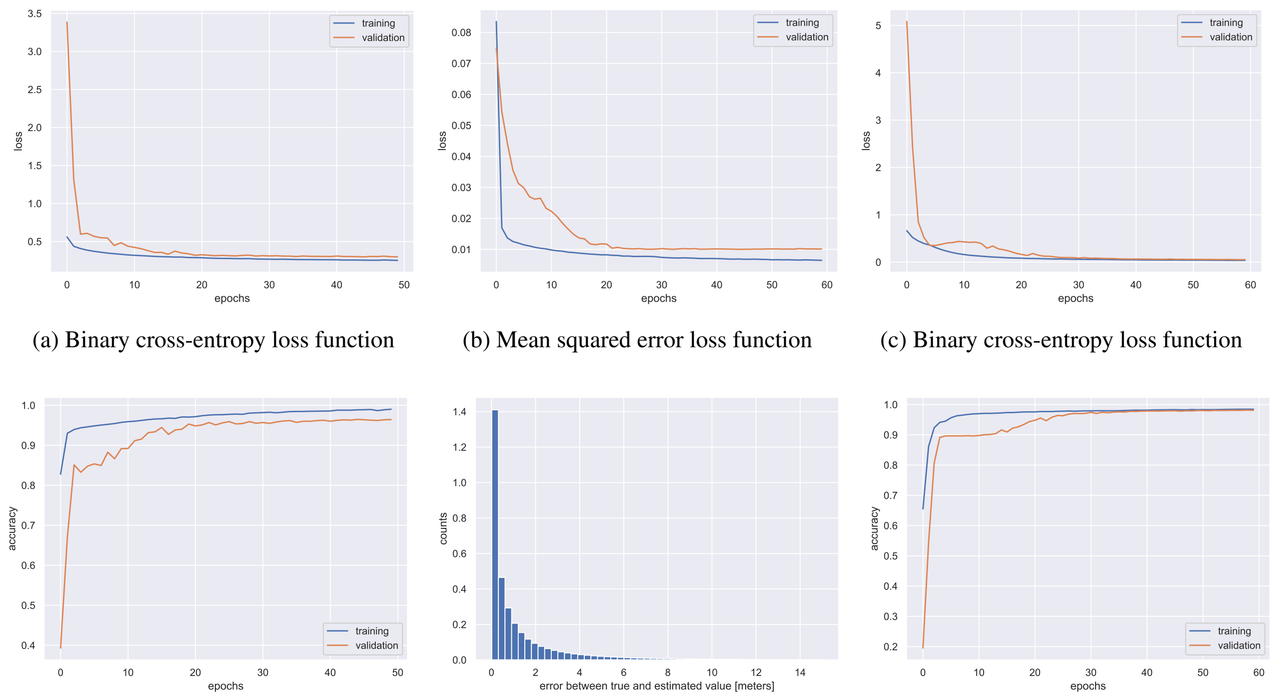

(a) Binary cross-entropy loss function
(b) Mean squared error loss function
(c) Binary cross-entropy loss function
(d) Accuracy plot
(e) Distribution of the height error
(f) Accuracy plot

Figure 7: Performances during training and validation for the three modules: (first column) vegetation detection, (second column) height estimation, (third column) building detection.

We note, from the sub-figures 7d and 7f, that the vegetation and building detection modules reach a validation accuracy of 96.4% and 98.1% respectively after 50 epochs. For the height estimation model, we calculate the distribution of the absolute error between the true and estimated height, $e = |y - \hat{y}|$ which shows a mean error of 1.4 meters (sub-figure 7e). Figure 8 shows some visual examples of the output of the different modules.

Once the models are trained, the corresponding outputs can be used to generate a risk map according to Equation 4. We extract several locations, spaced every 30 meters and covering the entire roadways. For the tree density and height calculations we extracted a window of 40 meters radius centered at each locations along the road while for the building density calculations we extracted a larger window of 150 meters. Figure 9 shows the risk map geographically displayed over the study area.

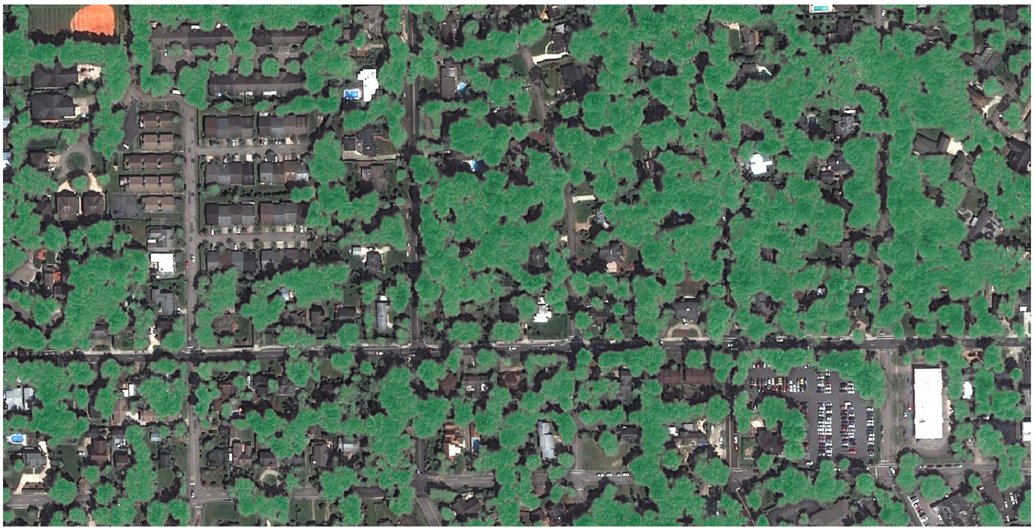

(a) Vegetation detection output

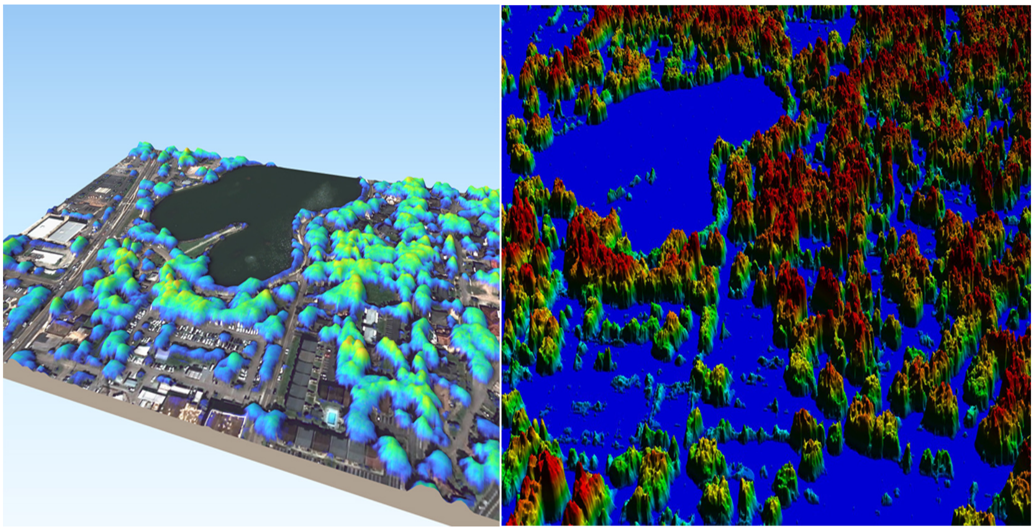

(b) Digital surface model generated from the satellite image by the second module of the framework

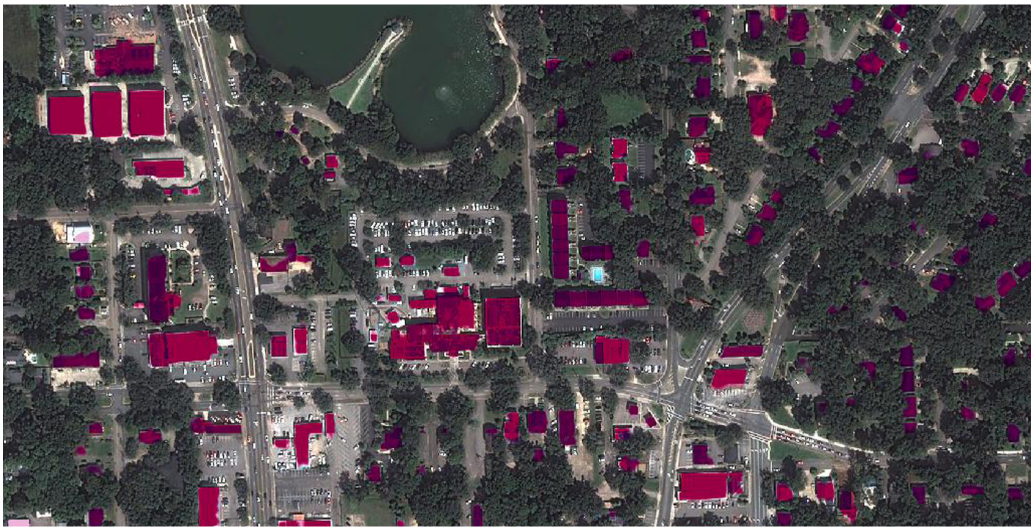

(c) Building detection output

Figure 8: Example of outputs of the three modules for a portion of the study area.

Figure 9: Risk map of the study area generated fully using our remote sensing approach. Risk values have been visually clusterized into three classes: green (low risk), orange (medium risk) and red (high risk).

It is possible to automatically highlight the most vulnerable locations at city scale. This can possibly help the management teams and city responders to organize and dislocate resources in specific points in the city. However, the proposed risk function is not unique and local authorities might implement customized, adapted risk functions. Furthermore, other data can be included into such a function. Nevertheless, in this paper the goal is to show the capabilities of remote sensing to retrieve useful information automatically that can be used for vulnerability assessment.

It is worth mentioning that some inherent limitations are present when working with optical satellite images. Clouds, in particular, can cover portions of the area, thus significantly affecting the quality of the image, as shown in Figure 10. Detection algorithms might not work properly in detecting trees or buildings.

Figure 10: Clouds and their corresponding shadows significantly reduce the view from optical satellite images

5 Conclusions and future works

In this paper, we developed an automated framework to detect vulnerabilities at roadway's level. We used a high-resolution satellite image of a portion of Tallahassee (Florida) acquired before Hurricane Michael. The framework consists of three different modules. The first detects vegetation characteristics, namely density and height. The second detects buildings using a semantic segmentation approach. Vegetation and buildings are combined together with road importance, which is here included as prior knowledge using a proposed risk function. The solution can generate a map of the areas showing the detected critical points. Such a map can be quickly generated before the event and can improve the planning procedures conducted by city and state agencies.

As future work, we aim to make the vulnerability assessment more robust, including more data or information. For example, automatic roadways detection can be performed, making the framework more applicable even when roadway shapefiles are not available.

6 Author Contributions

The authors confirm contribution to the paper as follows: study conception and design: M. Gazzea, A. Karaer, M. Ghorbanzadeh, E. E. Ozguven, and R. Arghandeh; analysis and interpretation of results: M.Gazzea, A. Karaer, M. Ghorbanzadeh and R. Arghandeh; manuscript preparation: M. Gazzea, A. Karaer, M. Ghorbanzadeh, E. E. Ozguven and R. Arghandeh. All authors reviewed the results and approved the final version of the manuscript.

References

[1] Jeffrey E Fulmer. What in the world is infrastructure? `https://30kwe1si3or29z2y020bgbet-wpengine.netdna-ssl.com/wp-content/uploads/2018/03/what-in-the-world-is-infrastructure.pdf`, 2009. [Online].

[2] Mahyar Ghorbanzadeh, Mohammadreza Koloushani, Mehmet Baran Ulak, Eren Erman Ozguven, and Reza Arghandeh Jouneghani. Statistical and spatial analysis of hurricane-induced roadway closures and power outages. *Energies*, 13(5):1098, Mar 2020.

[3] Michele Gazzea, Alican Karaer, Nozhan Balafkan, Eren Erman Ozguven, and Reza Arghandeh. Post-hurricanes roadway closure detection using satellite imagery and semi-supervised ensemble learning. In *Transportation Research Board 100th Annual Meeting 2021*, number TRBAM-21-00892, 2021.

[4] Michele Gazzea, Alican Karaer, Mahyar Ghorbanzadeh, Nozhan Balafkan, Tarek Abichou, Eren Erman Ozguven, and Reza Arghandeh. Automated satellite-based assessment of hurricane impacts on roadways. *IEEE Transactions on Industrial Informatics*, pages 1–1, 2021.

[5] D. Gullick, A. Blackburn, D. Whyatt, and P. Vopenka. Tree risk evaluation environment for failure and limb loss (treefall) : Predicting tree failure within proximity of infrastructure on an individual tree scale. 2017.

[6] Elnaz Kabir, Seth Guikema, and Brian Kane. Statistical modeling of tree failures during storms. *Reliability Engineering [?] System Safety*, 177:68–79, 09 2018.

[7] Cihan Çiftçi, S. Arwade, B. Kane, and S. Brena. Analysis of the probability of failure for open-grown trees during wind storms. *Probabilistic Engineering Mechanics*, 37:41–50, 2014.

[8] Jindong Wu. Developing general equations for urban tree biomass estimation with high-resolution satellite imagery. *Sustainability*, 11:4347, 08 2019.

[9] Martin Schaefer, Richard Teeuw, Simon Day, Dimitrios Zekkos, Paul Weber, Toby Meredith, and C.J. Westen. Low-cost uav surveys of hurricane damage in dominica: automated processing with co-registration of pre-hurricane imagery for change analysis. *Natural Hazards*, 101, 04 2020.

[10] Lake Singh, William Whittecar, Marc DiPrinzio, Jonathan Herman, Matthew Ferringer, and Patrick Reed. Low cost satellite constellations for nearly continuous global coverage. *Nature Communications*, 11, 01 2020.

[11] M. Gazzea, M. Pacevicius, D. O. Dammann, A. Sapronova, T. M. Lunde, and R. Arghandeh. Automated power lines vegetation monitoring using high-resolution satellite imagery. *IEEE Transactions on Power Delivery*, pages 1–1, 2021.

[12] S. Kaplan and B. Garrick. On the quantitative definition of risk. *Risk Analysis*, 1:11–27, 1981.

[13] E. Jenelius, T. Petersen, and L. Mattsson. Importance and exposure in road network vulnerability analysis. *Transportation Research Part A-policy and Practice*, 40:537–560, 2006.

[14] National Oceanic and Atmospheric Administration (NOAA). Catastrophic hurricane michael strikes florida panhandle october 10, 2018. `https://www.weather.gov/tae/HurricaneMichael2018`. [Online].

[15] U.S. Energy Information Administration. Hurricane michael caused 1.7 million electricity outages in the southeast united states. `https://www.eia.gov/todayinenergy/detail.php?id=37332`, 2018. [Online].

[16] Florida Forest Service. Initial value estimate of altered, damaged or destroyed timber in florida. `https://www.fdacs.gov/content/download/82204/file/HurricaneMichaelInitialTimberDamageEstimate1.pdf`, October 2018. [Online].

[17] National Center for Environmental Information. Assessing the u.s. climate in 2018. `AssessingtheU.S.Climatein2018`, 2018. [Online].

[18] Wikipedia contributors. Tallahassee, florida — Wikipedia, the free encyclopedia, 2021. [Online; accessed 22-July-2021].

[19] Ned Cake. Buildings footprint in leon county. `https://geodata-tlcgis.opendata.arcgis.com/datasets/tlcgis::buildings-2018/about`, January 2018. [Online].

[20] O. Ronneberger, P. Fischer, and T. Brox. U-net: Convolutional networks for biomedical image segmentation. *ArXiv*, abs/1505.04597, 2015.

[21] C. Xiao, R. Qin, X. Huang, and J. Li. Individual tree detection from multi-view satellite images. In *IGARSS 2018 - 2018 IEEE International Geoscience and Remote Sensing Symposium*, pages 3967–3970, 2018.

[22] H. Raggam. Surface mapping using image triplets: Case studies and benefit assessment in comparison to stereo image processing. *Photogrammetric Engineering and Remote Sensing*, 72:551–563, 2006.

[23] Henrik Persson, Håkan Olsson, M.J. Soja, L.M.H. Ulander, and Johan Fransson. Experiences from large-scale forest mapping of sweden using tandem-x data. *Remote Sensing*, 9:1253, 12 2017.

[24] A. Corte, F. E. Rex, D. Almeida, C. R. Sanquetta, C. A. Silva, Marks M. Moura, Ben Wilkinson, A. M. A. Zambrano, Ernandes M. da Cunha Neto, Hudson F. P. Veras, A. D. Moraes, Carine Klauberg, Midhun Mohan, A. Cardil, and E. N. Broadbent. Measuring individual tree diameter and height using gatoreye high-density uav-lidar in an integrated crop-livestock-forest system. *Remote. Sens.*, 12:863, 2020.

[25] Michele Gazzea, Sindre Aalhus, Lars Kristensen, Eren Ozguven, and Reza Arghandeh. Automated 3d vegetation detection along power lines using monocular satellite imagery and deep learning. In *IGARSS 2021 - 2021 IEEE International Geoscience and Remote Sensing Symposium*, 2021.

[26] K. He, X. Zhang, S. Ren, and J. Sun. Deep residual learning for image recognition. In *2016 IEEE Conference on Computer Vision and Pattern Recognition (CVPR)*, pages 770–778, 2016.